



HAL
open science

Progress in the development of a versatile ZDES-based methodology for aerospace flows

Pierre-Elie Weiss, Sebastien Deck

► **To cite this version:**

Pierre-Elie Weiss, Sebastien Deck. Progress in the development of a versatile ZDES-based methodology for aerospace flows. AERO 2020+1 - 55th 3AF International Conference on Applied Conference, Apr 2021, Poitiers (virtuel), France. hal-03206316

HAL Id: hal-03206316

<https://hal.science/hal-03206316>

Submitted on 23 Apr 2021

HAL is a multi-disciplinary open access archive for the deposit and dissemination of scientific research documents, whether they are published or not. The documents may come from teaching and research institutions in France or abroad, or from public or private research centers.

L'archive ouverte pluridisciplinaire **HAL**, est destinée au dépôt et à la diffusion de documents scientifiques de niveau recherche, publiés ou non, émanant des établissements d'enseignement et de recherche français ou étrangers, des laboratoires publics ou privés.

Progress in the development of a versatile ZDES-based methodology for aerospace flows

P.-E. Weiss⁽¹⁾ and S. Deck⁽¹⁾

⁽¹⁾DAAA, ONERA, Université Paris Saclay, F-92190 Meudon - France, peweiss@onera.fr

ABSTRACT

In the aerospace field, a growing need for reactivity has arisen due to the competition in the design of new space launchers such as reusable launch vehicles. In this context, the development and the validation of advanced numerical strategies is of primary importance to allow the quantitative simulation of the physical phenomena driving the multi-scale physics of turbulent flows around complex geometries. The present paper aims to illustrate the use of an innovative numerical framework denoted as Zonal Immersed Boundary Conditions (ZIBC) [10], [21] to unveil the salient unsteady features of a sub-scale Ariane 6 PPH model. The numerical strategy allowing the coupling between a modelling method (e.g. RANS, URANS, ZDES, LES or DNS) and IBC (Immersed Boundary Conditions) is reminded. The high level of maturity of the Zonal Detached Eddy Simulation (ZDES) [2, 4] is presently used in the ZIBC strategy for the prediction of turbulent separated flows and permits to simulate complex configurations dealing with internal or external aerodynamics. A deep physical analysis based on single- and two-point spectra reveals an a priori unexpected change of phenomenology comparing the configuration of interest for two transonic Mach numbers namely $M_\infty = 0.7$ and 0.9 with the same angle of attack equal to -3° . In particular, the PSD of the normal force coefficient integrated from the nose to the base (which is excluded) of the configuration clearly illustrates that the flow dynamics is driven by phenomena related to one and two characteristic frequencies for $M_\infty = 0.7$ and 0.9 , respectively.

1. INTRODUCTION

In the frame of the design of space launchers, a major point of interest for the aerodynamics concerns the pe-

riod of the flight during which the transition from transonic to supersonic regimes occurs when a maximum of dynamic pressure is reached. In this phase, it is mandatory to be able to assess the unsteady efforts exerted upon the launcher when both the Mach number and the angle of attack change. On the numerical side, a direct involvement is the need to build a versatile methodology which allows computing the compressible turbulent flows developing around arbitrary space vehicle shapes. To do so, a numerical workflow denoted as ZIBC (Zonal Immersed Boundary Conditions) has been designed and validated [21, 10, 8, 9]. The present work constitutes the continuation of the study presented by Weiss [22] which provided a preliminary overview of the numerical reproduction of the flow developing on an intermediate Ariane 6 configuration named PPH (i.e. made up with a first stage of three P145 rocket motors, a second stage with a single P145 rocket motor, and a H32 cryogenic upper stage). For this specific configuration, an a priori unexpected unsteadiness was revealed during ONERA's S2MA experiments. The purpose of the present paper is to propose an explanation to this unsteady phenomenon relying on the ZIBC strategy which was successfully used to predict the buffeting phenomenon on a complete Ariane 5 configuration. The paper is organised as follows: section 2 presents the main features of the Ariane 6 PPH case; section 3 describes the preprocessing step needed to use ZIBC; section 4 is divided into sub-section 4.1 which reminds and extends the results presented in [22] for two Mach numbers namely 0.7 and 0.9 with an incidence equal to -3° and sub-section 4.2 which is focused on the spatial organisation of the fluctuating pressure field and the characteristic frequencies of the unsteady loads.

2. TEST CASE

The studied configuration consists in a former version of the future Ariane 6 space launcher represented in figure 1. In this figure, the test case of interest is split into a central main stage (CC) and two boosters (PAP1 and PAP2) linked by two series of struts. The forward struts link the nose cones of the boosters to the main stage. Downstream, the aft struts attach the afterbody bases together. Finally, it has to be noticed that the sting holding the model is also computed to ensure the representativeness of the blockage effect occurring in the wake.

The two transonic Mach numbers of interest namely $M_\infty = 0.7$ and $M_\infty = 0.9$ are denoted in the following as *M07* and *M09*, respectively. The configuration is inclined by an angle $\alpha = -3^\circ$ meaning that the flow arrives on the top of the fairing. The main parameters of the configuration related to the investigated Mach numbers such as the static and stagnation quantities and the characteristic sizes of the geometry are gathered in table 1.

| Test case | M07 | M09 |
|-----------------------------|---------|---------|
| M_∞ (-) | 0.7 | 0.9 |
| p_∞ (Pa) | 169468 | 109417 |
| T_∞ (K) | 282.6 | 268.1 |
| p_i (Pa) | 235000 | 185000 |
| T_i (K) | 310 | 311 |
| α (deg) | -3 | -3 |
| q_∞ (Pa) | 58128 | 62045 |
| $Re_{L_{ref}}$ (-) | 3019612 | 2683383 |
| S_{ref} (m ²) | 0.00916 | 0.00916 |
| $L_{ref} = D$ (m) | 0.108 | 0.108 |
| d (m) | 0.07 | 0.07 |

Table 1: Geometrical and physical parameters

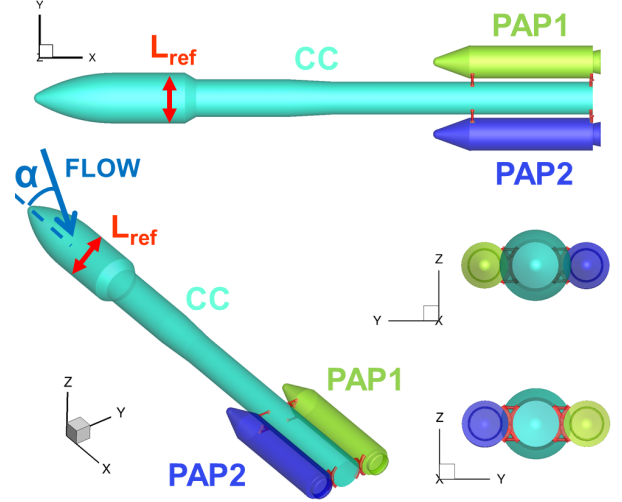


Figure 1: Geometry of the main central body (CC) along with the boosters (PAP1 and PAP2). The forward and aft struts are represented in red.

3. NUMERICAL SET-UP

Given the low incidence of the configuration (i.e. $\alpha = -3^\circ$) a common structured multi-block grid (see figure 2) containing 164 blocks and 270×10^6 points is built for both Mach numbers. The freestream conditions lead to close values of the first cell size Δy_0 in the wall normal direction for the two Mach numbers namely $\Delta y_{0,M07} = 10^{-6}$ m and $\Delta y_{0,M09} = 1.26 \cdot 10^{-6}$ m with respect to the classical criterion for the dimensionless first cell size $y^+ = 1$. Thus, the lowest cell size is chosen to permit the generation of a unique mesh. The background grid made in the view of the local introduction of immersed boundary conditions is generated using three O-H topologies (i.e. one for the main stage and two for the boosters) which avoids singularity issues near the axes of each cylindrical body. The resulting mesh clusters 360 points in azimuth due to the major role played by the spatial organisation for the azimuthal modes [23, 3, 16, 14] in the flow dynamics. In addition, the confined area between the main stage and the boosters is refined as recommended in former studies [13, 19, 20]. The whole computational domain consists in a cylinder with a circular section with more than $200d$ (with d the smallest diameter of the main stage) in each direction to avoid any reflections of spurious numerical waves. In this domain, the boosters and the main stage are meshed in a body-fitted manner whereas the struts are introduced in the background grid using zonal immersed boundary conditions due their complex shape as shown in figure 3. In practice, the immersed boundary method consists in adding body forces in a continuous or discrete manner to mimic classical boundary conditions (e.g. adiabatic

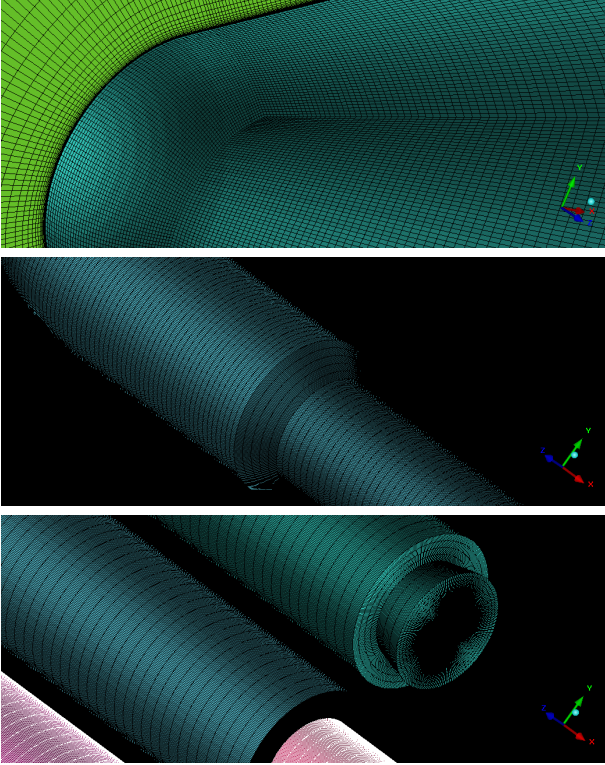


Figure 2: (From top to bottom) Views of the mesh near a booster nose, the fairing boat-tail section, the launcher afterbody hold by a sting.

or isothermal walls, slip or no-slip conditions, porosity, etc ...). In the present work the continuous form of the compressible Navier-Stokes equations including the ZDES and IBC source terms is summarised. Then, for the sake of brevity, the discrete version of this system, which is implemented in practice, can be found in details in Weiss and Deck[21] for the finite volume approach in the same spirit as in Mohd-Yusof [11] for a spectral approach or Verzicco *et al.* [15] and Fadlun *et al.* [5] for a finite-difference-based LES. In this reference[21], the source terms related to the ZDES and the IBC are clearly highlighted in the description of the formulation by the notations $\mathbf{T}_{\text{ZDES}}^{(1)}$ and $\mathbf{T}_{\text{IBC}}^{(2)}$, respectively. It can be noticed that a tagging procedure has to be performed distinguishing solid cells from fluid cells. This permits to obtain values of tag_{IBC} which correspond to α_{IBC} in the discrete form of the source term $\mathbf{T}_{\text{IBC}}^{(2)}$ and act as a sensor that reads as 1 or 0 depending if the cell center is inside or outside the immersed object, respectively. A major difference exists between α_{IBC} and tag_{IBC} . α_{IBC} can be equal to 1 in a part of a cell and equal to 0 in the remaining volume of the same cell. On the contrary, each cell has a value of 0 or 1 for the marker tag_{IBC} . In the frame of the Spalart-Allmaras model and thus of ZDES, the accurate calculation of the

distance to the wall d_w is crucial. As mentioned before, the use of immersed boundary conditions requires a pre-processing step to distinguish fluid cells (i.e. outside the bodies) from solid cells (i.e. inside the bodies) using a raytracing algorithm such as the one described by O'Rourke [12] from the knowledge of the surface of the technological details which can be made of triangles as in a STL (STereo-Lithography) CAD file. Following the immersion of the object, an update of the wall distance computation has to be performed when a turbulence model needs it (e.g. the Spalart-Allmaras model) as described in Mochel *et al.* [10]. In the frame of the use of Immersed Boundary Conditions, the most automated mode of ZDES namely mode 2 is well-adapted to predict separations for configurations with high pressure zones and velocity fluctuations downstream.

We have implemented the original IB method (i.e. direct forcing) in two industrial flow solvers namely FLU3M [6] and ONERA's elsA software [1]. Both codes are based on second-order accurate time and space schemes. The calculations presented in this paper are performed with the FLU3M code. This code solves the Navier-Stokes equations with a low-dissipation AUSM+(P) convective scheme [7] on multi-block structured grids without limiter for the M07 case and with a minmod limiter for the M09 case for robustness purposes. The time integration is carried out by means of an implicit second-order accurate backward scheme. The simulation was realised on 396 Broadwell cores. The preprocessing needed by the IBC to distinguish mesh cells with a fluid or solid tag is realized by the external program RAYTRACER3D [10]. The resulting wall distance based on the knowledge of this fluid/solid interface is represented in figure 3.

4. RESULTS AND DISCUSSION

4.1 Instantaneous flowfield and time-averaged statistics

The observation of the instantaneous flow field permits to evidence qualitatively the spatial organisation of the coherent structures of the turbulent flow. Figure 4 shows the iso-contours of the density gradient norm in plane aligned with the boosters (B) and normal to the boosters (NB) for the M07 configuration. Such a plot illustrates the wide range of turbulent scales in the flow resolved and convected over a large distance from the nose to the tail of the configuration. In particular, downstream the separation at the nose fairing rear cone, a shear layer develops with a pairing process of the turbulent structures similar to the one observed for a canonical axisymmetric mixing layer. Then, hairpin-like structures occur and propagate until meeting the conical nose of the boosters and the for-

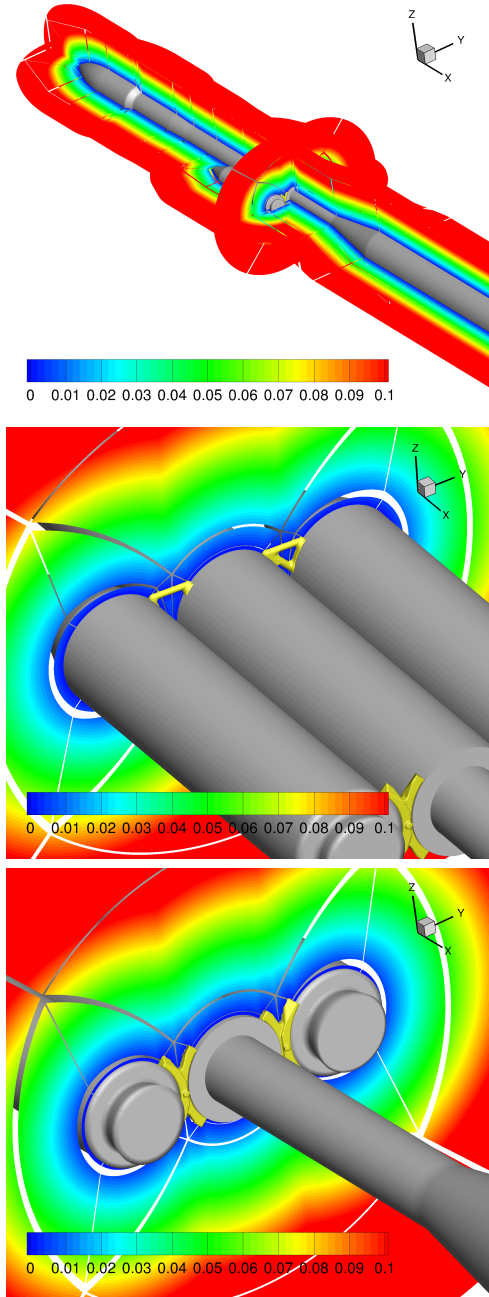


Figure 3: (From top to bottom) Global visualisation and local views near the forward and aft struts of the wall distance iso-contours.

ward struts. Finally, the flow separates again reaching the launcher afterbody and the resulting wake is partially stabilised by the presence of the sting. The M_{09} case which is not represented here presents a similar organisation along with expansion waves and shock waves at the nose of each cylindrical body interacting with the forward struts.

Prior to advanced physical analysis of the unsteady phenomena occurring in the flow, the ZDES results are

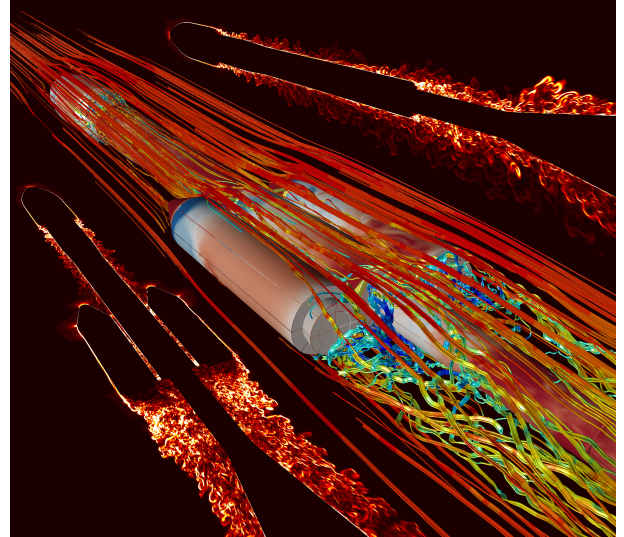


Figure 4: Iso-contours of instantaneous wall pressure and streamlines coloured by the instantaneous values of the streamwise velocity component for the M_{07} case. In the background, iso-contours of the density gradient norm are shown for two slices corresponding to a $(x-y)$ plane at $z=0$ and a $(x-z)$ plane at $y=0$.

validated using the available PSP (Pressure Sensitive Paint) experimental data. The time-averaged statistics are computed directly during the numerical simulation. The mean pressure coefficient ($\overline{C_p}$) is represented at the wall and compared with the pressure field obtained during ONERA's S2MA test campaign using PSP for both Mach numbers in figures 5 and 6. At first sight, the distribution of the mean pressure coefficient at the suction side seems to be similar for $M_\infty = 0.7$ and $M_\infty = 0.9$. High pressure zones are located in the neighbourhood of the booster noses followed by low pressure zones surrounding the fairing of the strap-on booster. Downstream the separation occurring on the nose fairing rear cone a recompression area can be noticed. Then, due to a slight decrease of the main stage diameter, a low pressure area forms before the flow enters the confinement zone limited by the forward struts linking the boosters to the main stage. The most salient discrepancies in terms of $\overline{C_p}$ levels between the two Mach numbers of interest come from the shock waves located near the middle of the main stage fairing and at the base of the conical noses of the auxiliary boosters. These normal shock waves contribute to the spatial extent of the high pressure zones.

An overall good agreement between the pressure field of the ZDES simulations and the PSP fields is obtained. In particular, the characteristic pressure discontinuities at the wall due to the presence of the shock waves are reproduced. The overpressure areas near the confined flow regions and close to the noses of the main stage and the

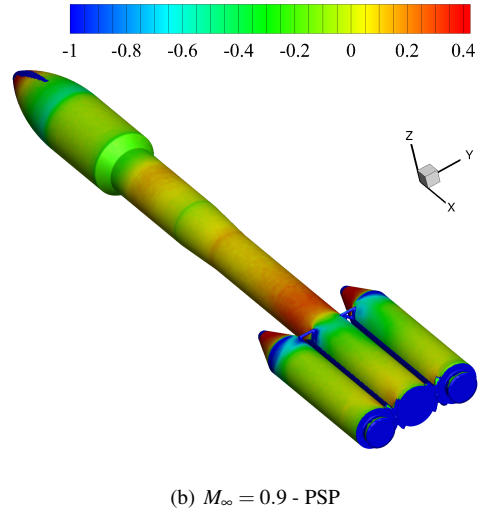
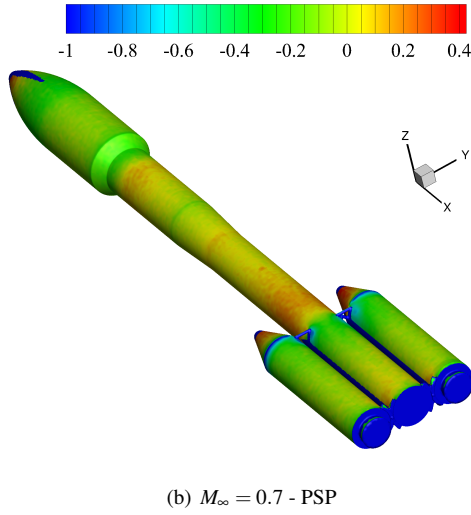
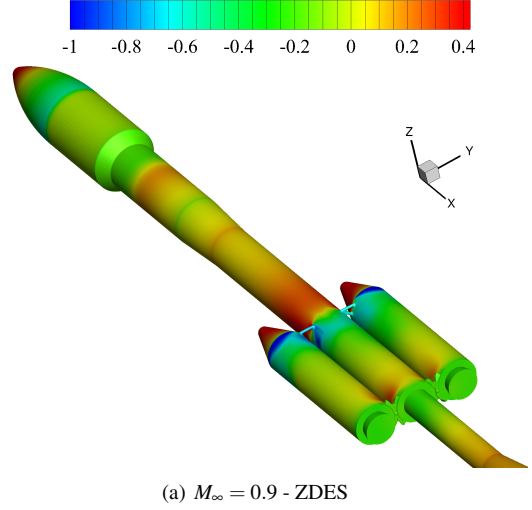
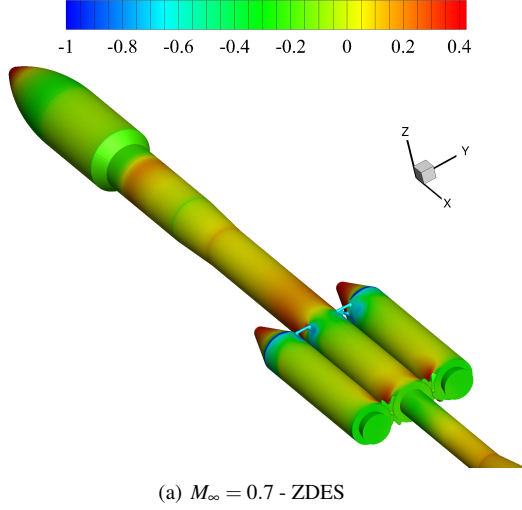


Figure 5: Iso-contours of the mean pressure coefficient $\overline{C_p}$ at the suction side for case $M07$

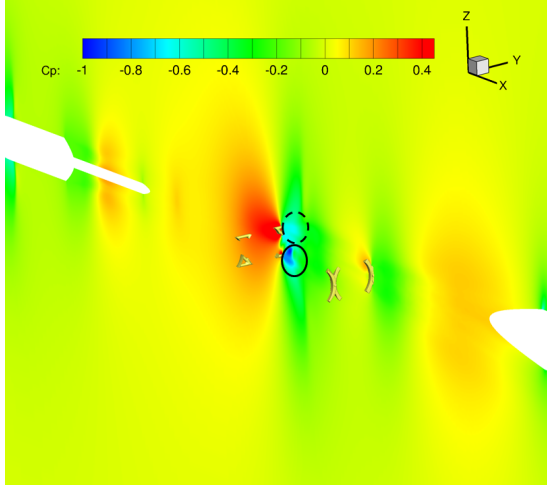
Figure 6: Iso-contours of the mean pressure coefficient $\overline{C_p}$ at the suction side for case $M09$

boosters are also observed. Moreover, for the $M09$ case, expansion waves on the boosters are well reproduced. Concerning the location of the reattachment points of the recirculation bubbles, some differences exist for the $M09$ case. Indeed, the length of the recirculation zone in the simulation approximately equal to $0.7L_{ref}$ is overestimated with respect to the one obtained with PSP data ($\sim 0.6L_{ref}$). For the $M07$ configuration, the length of the recirculation zone which is almost equal to $0.5L_{ref}$ in the experiments is properly reproduced by the ZIBC simulation.

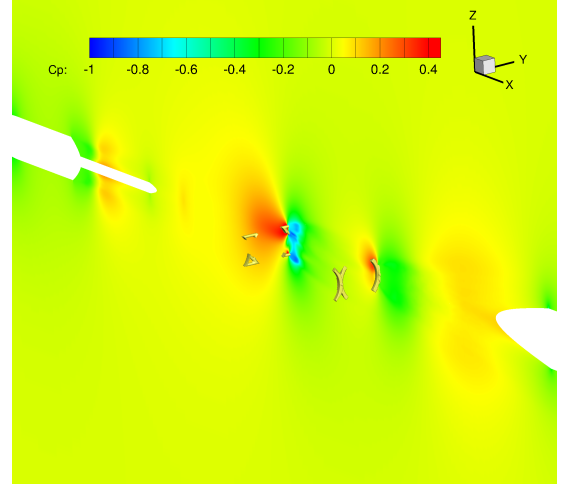
Iso-contours of $\overline{C_p}$ levels shown in figures 8 and 7 between the boosters and the main stage clearly evidence the strong overpressure area upstream from the struts illustrating the significant blockage effect they constitute for the flow. Downstream the forward asymmetric struts, a similar observation can be done for the velocity field

in the separated flow. Indeed, for the case $M_\infty = 0.7$, two low pressure zones can be distinguished. They appear symmetrical with respect to the $(x - y)$ plane in any plane between a booster and the main stage (i.e. planes located at $y = -0.35L_{ref}$ or $y = +0.35L_{ref}$). For the $M09$ case with a higher Mach number, the observation differs. In planes between a booster and the main stage, a clear asymmetry of the spatial organisation of the mean pressure field is revealed with respect to plane $(x - y)$. Such a pressure distribution presenting alternate zones of low and high pressure with respect to plane $x0y$ reminds the ones previously identified with the ZDES simulation of a full Ariane 5 configuration with similar asymmetric struts ([17],[18],[19],[20],[21]). These ZDES computations permitted to unveil a solid rotation of the flow with a loss of planar symmetry leading to additional side loads.

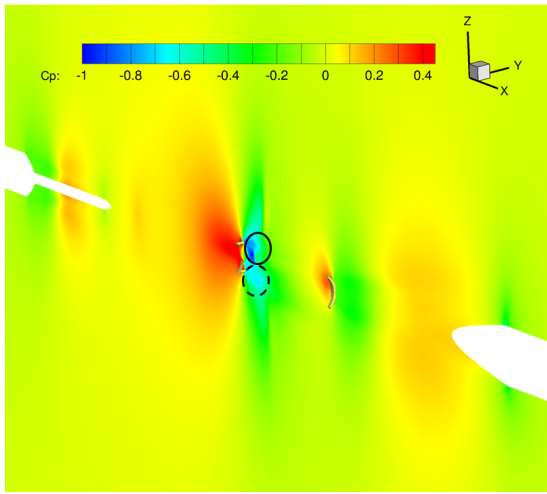
Although the first-order statistics tend to a symmetrical



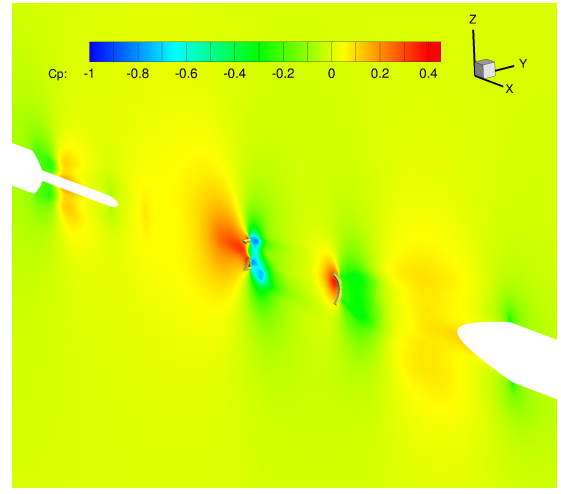
(a) $M_\infty = 0.9$ - plane between CC and PAP1



(a) $M_\infty = 0.7$ - plane between CC and PAP1



(b) $M_\infty = 0.9$ - plane between CC and PAP2



(b) $M_\infty = 0.7$ - plane between CC and PAP2

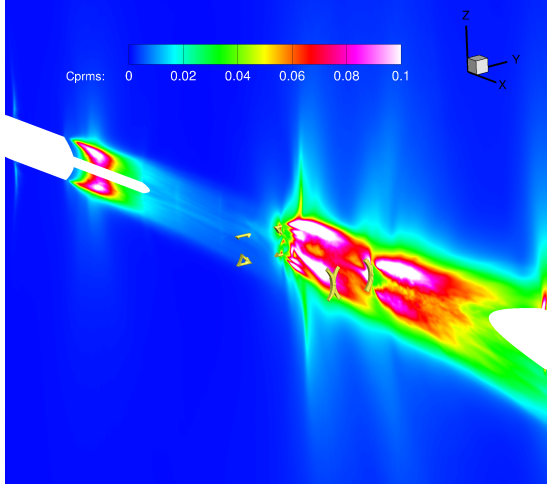
Figure 7: Iso-contours of the mean pressure coefficient \overline{Cp} in two longitudinal planes between the strap-on boosters and the main stage at $y = -0.35L_{ref}$ (left) and $y = +0.35L_{ref}$ (right).

Figure 8: Iso-contours of the mean pressure coefficient \overline{Cp} in two longitudinal planes between the strap-on boosters and the main stage at $y = -0.35L_{ref}$ (left) and $y = +0.35L_{ref}$ (right).

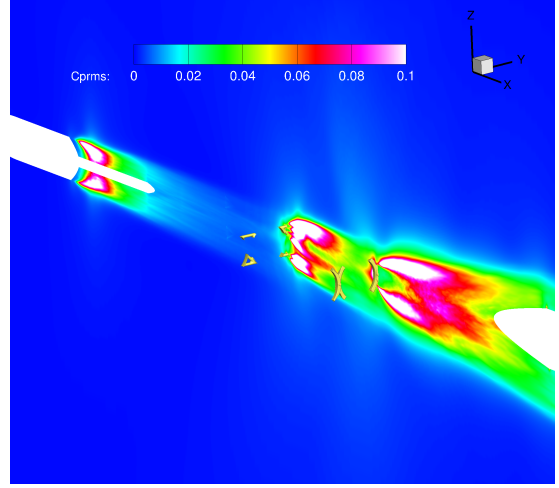
distribution for both Mach numbers, it is not necessarily the case for the spatial organisation of the fluctuating field. Iso-contours of the fluctuating pressure coefficient Cp_{rms} are represented at the wall for cases *M07* and *M09* in figures 10 and 9, respectively. This second-order statistical moment for the time signal of pressure is defined by $Cp_{rms} = \overline{p'}/\frac{1}{2}\rho_\infty U_\infty^2$ where $\overline{p'}$ corresponds to the *rms* fluctuating pressure. For the *M09* configuration, a strong asymmetry has been observed in [22] comparing the patterns of the areas in which the wall *rms* pressure reaches a maximum, at the suction side near the boosters (i.e. for positive z). At the opposite, the wall signature of the fluctuating pressure for both configurations *M07* and *M09* tends to remain symmetrical at the pressure side in the neighbourhood of the boosters (i.e. for

negative z). This major discrepancy between $M_\infty = 0.7$ and $M_\infty = 0.9$ suggests that each transonic case has its own flow dynamics. Moreover, at the junction between the conical nose and the cylinder of the boosters, a strong oscillation of the shock waves is revealed by the highest values of the fluctuating pressure at the wall forming oblique patterns ([22]). This intermittency of the expansion wave and the shock system is also visible in the field in figure 9. Finally, the aft struts attached at the afterbody base constitute a very significant blockage effect for the upcoming flow. As a consequence, the flow near these attached devices exhibit higher Cp_{rms} values than those observed around the forward struts.

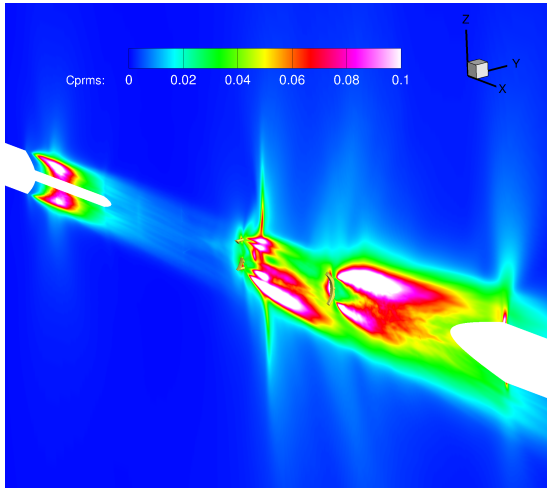
The very confined areas in the Ariane 6 PPH config-



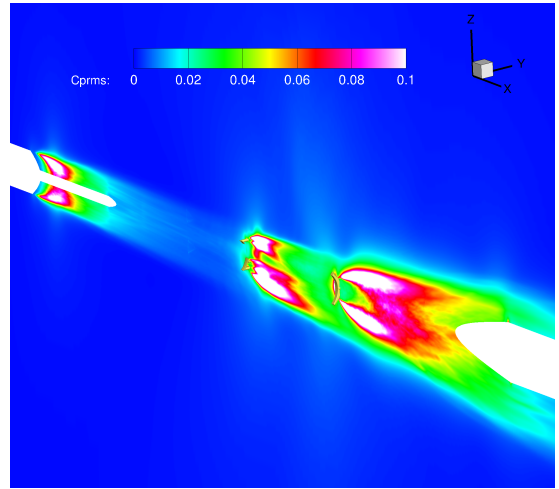
(a) $M_\infty = 0.9$ - plane between CC and PAP1



(a) $M_\infty = 0.7$ - plane between CC and PAP1



(b) $M_\infty = 0.9$ - plane between CC and PAP2



(b) $M_\infty = 0.7$ - plane between CC and PAP2

Figure 9: Iso-contours of the fluctuating pressure coefficient Cp_{rms} in two longitudinal planes between the strap-on boosters and the main stage at $y = -0.35L_{ref}$ (left) and $y = +0.35L_{ref}$ (right).

uration could explain the occurrence of unsteady phenomena for $M_\infty = 0.9$ only. Indeed, the closeness of $M_\infty = 0.9$ to the sonic Mach number is sufficient to establish an oscillating system with shock and expansion waves which is not the case for a lower Mach number such as $M_\infty = 0.7$. The location of the reattachment point on the main stage after the impingement of the axisymmetric mixing layer evolves with time and leads to an intermittent phenomenon. The axisymmetric shear layers also existing in the afterbody region of the launcher limit the spatial extent related to the breathing phenomenon of the recirculation bubbles. These oscillatory movements potentially interact with the *buffet* phenomenon (resembling to the one occurring on nacelles or wings of aircraft) of the shock and expansion waves located at the base of the

Figure 10: Iso-contours of the fluctuating pressure coefficient Cp_{rms} in two longitudinal planes between the strap-on boosters and the main stage at $y = -0.35L_{ref}$ (left) and $y = +0.35L_{ref}$ (right).

conical nose of the strap-on boosters. This phenomenon has to be distinguished from the *buffeting* phenomenon at the base of launchers. The interaction of these unsteady phenomena happens in particularly confined areas with a strong blockage effect of the struts around the afterbody bases (i.e. those of the boosters and the main stage). Then, it seems that when the flow becomes nearly sonic going from $M_\infty = 0.7$ to $M_\infty = 0.9$ an instability with an intrinsic dynamics appears.

4.2 Spectral analysis

PSD plots $f.G(f)_{C-}$ of the integrated loads along the launcher (bases and sting excluded) are proposed as a function of the frequency in figures 11, 12, 13 for both

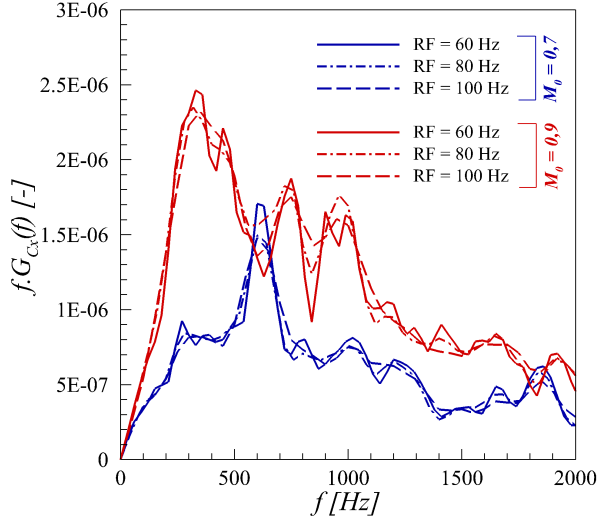


Figure 11: PSD of the axial force coefficient for two Mach numbers (i.e. $M_\infty = 0.7$ and 0.9) and three frequency resolutions (i.e. $RF = 60, 80, 100$ Hz).

Mach numbers of interest ($M_\infty = 0.7$ and 0.9). The PSD of the side load coefficient CY presents several harmonics of the fundamental frequency equal to 250 Hz which corresponds to harmonics of the Strouhal number $f \cdot D / U_\infty \cdot \cos \alpha = 0.1$ for the case $M09$. The dimensionless Strouhal number $St_D = 0.1$ based on the reference length ($L_{ref} = D$) is found on the spectrum of the axial force coefficient CA . The case $M07$ does not represent such a clear set of harmonics and the flow dynamics seems to be dominated for the CA coefficient by a frequency centred around $St_D = 0.3$. On the normal force coefficient CN in the model reference frame, two distinct dynamics are found for the flow driven by a unique frequency $St_D = 0.23$ ($f = 500$ Hz) for the case $M07$ and two frequencies $St_D = 0.065$ ($f = 150$ Hz) and $St_D = 0.25$ ($f = 670$ Hz) for the case $M09$.

To get further into the spatial organisation of the fluctuating pressure field, one can get interested in the azimuthal coherence of two pressure sensors $p_1(t, \phi_1)$ and $p_2(t, \phi_2)$ located at the surface of the launcher. The wall pressure field being intrinsically 2π -periodic on the center body, the real part of the coherence function $C_r(f, \Delta\phi)$ can be decomposed into Fourier modes as follows:

$$C_r(f, \Delta\phi) = \sum_m C_{r,m} \cos(m\Delta\phi) \quad (1)$$

where $C_{r,m}$ stands for the percentage of fluctuating energy at a frequency f related to the azimuthal mode m given $\sum_m C_{r,m} = 1$. Azimuthal modes $m = 0, 1, 2$ correspond to the axisymmetric, antisymmetric (generating side loads) and ovalisation mode, respectively. Looking at the spectra for the three first azimuthal modes at Mach numbers $M_\infty = 0.7$ and 0.9 for 9 rings of sensors dis-

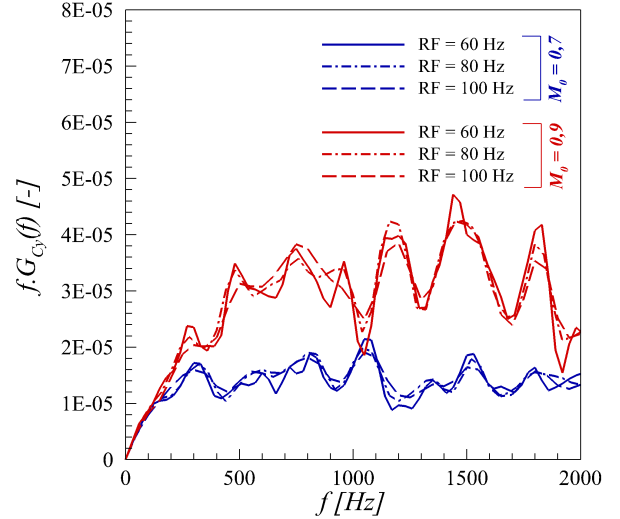


Figure 12: PSD of the side force coefficient for two Mach numbers (i.e. $M_\infty = 0.7$ and 0.9) and three frequency resolutions (i.e. $RF = 60, 80, 100$ Hz).

tributed along the main stage, it is possible to notice that rings located just downstream the fairing, the antisymmetric mode $m = 1$ contains almost 50% of the energy of the fluctuations. In the case $M_\infty = 0.7$, the contribution to mode $m = 1$ is particularly remarkable for ring 2200 located at the afterbody base where mode $m = 1$ contributes to nearly 70% of the energy of the fluctuations at a frequency centred around 550 Hz. A similar behaviour is observed for $M_\infty = 0.9$. Indeed, the figure 14 presents the contribution of mode $m = 1$ for rings 700, 1800 and 2200 distributed along the main stage at the fairing boat-tail section, behind the booster noses and at the afterbody base, respectively. Such a plot illustrates the contribution of the frequency $St_D = \frac{fD}{U_0 \cos(\alpha)} \approx 0.2$ for both studied Mach numbers. The case $M_\infty = 0.9$ is singular due to the significant contribution to the total energy of the lowest frequencies i.e. $St_D \leq 0.1$ which could be associated to the shock unsteadiness as indicated in figure 9 showing the *rms* fluctuations in the field surrounding the launcher.

5. CONCLUSION

The present study was devoted to the study of the unsteady aerodynamics of an Ariane 6 PPH configuration using Zonal Immersed Boundary Conditions. Following the description of the geometry, the generation of the topology of the grid and the numerical methods used in the study have been presented. In particular, the preprocessing step allowing the tag of the grid cells and the computation of the wall distances for the configuration Ariane 6 PPH which is mandatory to the use of an immersed boundary method have been detailed. The

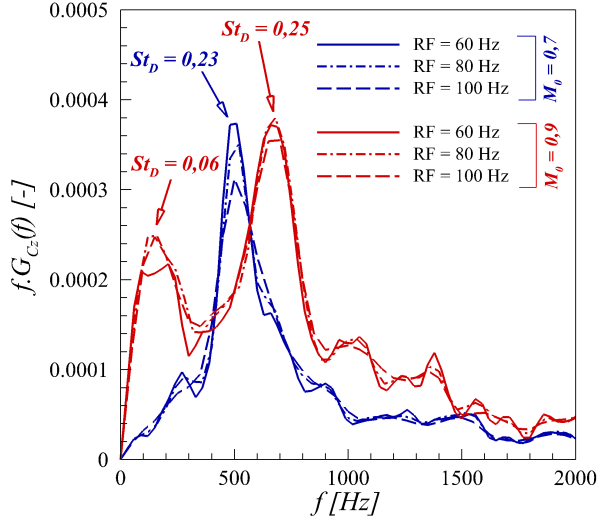


Figure 13: PSD of the normal force coefficient for two Mach numbers (i.e. $M_\infty = 0.7$ and 0.9) and three frequency resolutions (i.e. $RF = 60, 80, 100$ Hz).

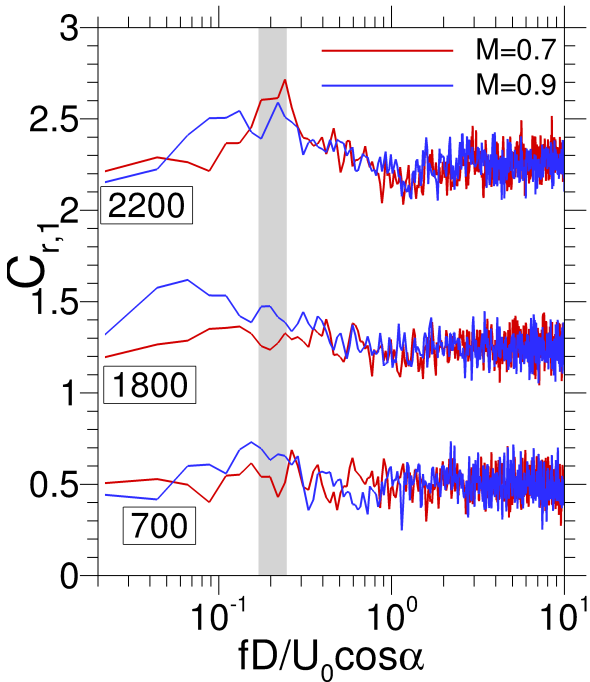


Figure 14: Spectra of the antisymmetric mode $m = 1$ for $M_\infty = 0.7$ and 0.9 as a function of $\frac{fD}{U_0 \cos(\alpha)}$.

coupling of the ZDES approach and the IBC method using the FLU3M code has been reminded. Finally, the outputs of the simulation defined to correspond to the location of the experimental sensors and allowing the physical analysis of the unsteady phenomena of interest have been presented. Results from ZDES simulations

have been shown for both Mach numbers. The comparison of the computations with available experimental data has permitted to show a good agreement regarding the spatial distribution and the magnitude of the mean pressure levels with the experimental field obtained with the PSP technique.

A deeper analysis of the instantaneous, time-averaged and fluctuating fields has suggested a physical interpretation of the observed unsteady phenomena. The case at $M_\infty = 0.7$ seems to be dominated by a unique dimensionless frequency $St_D = 0.2$ associated to a mode $m = 1$ whose correlation reaches a maximum near the aft struts downstream which a recirculation area develops. This configuration, as for the case at $M_\infty = 0.9$, presents some similarities with the flow dynamics classically obtained downstream an axisymmetric backward-facing step which can be due to the forebody geometry. The case $M09$ is singular due to the occurrence of shock and expansion wave systems strongly oscillating in the neighbourhood of the forward struts. These asymmetric struts which are very close to the shape of the aft struts of the Ariane 5 launcher seem to create a solid rotation of the flow revealed by the alternate pattern of low pressure values visible on the mean pressure coefficient iso-contours, able to sustain a secondary recirculation zone. Such a phenomenon does not exist for the case $M07$ whose flow dynamics is mostly associated to the development of mixing layers in the aft strut region. The occurrence of these two recirculation zones downstream of each attached devices might be related to the existence of the two characteristic frequencies observed. It is interesting to note that this investigation illustrates the capacity of the coupled ZDES/IBC approach to take into account complex geometries which can be used to simulate the unsteady aerodynamics of conventional and reusable space vehicles. Such a method permits to perform a deep analysis of the unsteady flow in the context of risk removal calculation for critical points in the timeline of the flight of a launcher without simplifications on the computed geometry.

6. ACKNOWLEDGMENTS

The Centre National d'Études Spatiales (CNES) is particularly acknowledged for funding the numerical activities related to the afterbody cases with struts and with all technological details modelled using the ZIBC approach developed in the frame of the research project ALLIGATOR funded by ONERA.

REFERENCES

- [1] L. Cambier, S. Heib, and S. Plot. The Onera elsA CFD Software: Input from Research and

- Feedback from Industry. *Mechanics and Industry*, 14(3):159,174, 2013.
- [2] S. Deck. Recent improvements in the Zonal Detached Eddy Simulation (ZDES) formulation. *Theoretical and Computational Fluid Dynamics*, 26(6):523–550, 2012.
- [3] S. Deck and P. Thorigny. Unsteadiness of an axisymmetric separating-reattaching flow. *Physics of Fluids*, 19(065103), 2007.
- [4] S. Deck, P.-E. Weiss, and N. Renard. A rapid and low noise switch from RANS to WMLES on curvilinear grids with compressible flow solvers. *Journal of Computational Physics*, 363:231–255, 2018.
- [5] E. A. Fadlun, R. Verzicco, P. Orlandi, and J. Mohd-Yusof. Combined Immersed-Boundary/Finite-Difference Methods for Three-Dimensional Complex Flow Simulations. *Journal of Computational Physics*, 161(1):35–60, 2000.
- [6] P. Guillen and M. Dormieux. Design of a 3D multi-domain Euler code. In *International Seminar of Supercomputing*, Boston, USA, 1989.
- [7] M. S. Liou. A sequel to AUSM : AUSM+. *J. Comp. Phys.*, 129:364–382, 1996.
- [8] L. Manueco, P.-E. Weiss, and S. Deck. Towards the Prediction of Fluctuating Wall Quantities Using Immersed Boundary Conditions. *AIAA Aviation, Dallas, USA, 17-21 June*, 2019.
- [9] L. Manueco, P.-E. Weiss, and S. Deck. On the estimation of unsteady aerodynamic forces and wall spectral content with immersed boundary conditions. *Computers & Fluids*, 201:104471, April 2020.
- [10] L. Mochel, P.-E. Weiss, and S. Deck. Zonal Immersed Boundary Conditions: Application to a High-Reynolds-Number Afterbody Flow. *AIAA Journal*, 52(12):2782–2794, 2014.
- [11] J. Mohd-Yusof. Combined immersed-boundary/b-spline methods for simulations of flows in complex geometries. *Annual Research Briefs, Center for Turbulence Research*, pages 317–328, 1997.
- [12] J. O’Rourke. *Computational geometry in C*, Second Edition. Cambridge University Press, 1998.
- [13] R. Pain, P.-E. Weiss, and S. Deck. Zonal Detached Eddy Simulation of the flow around a simplified launcher afterbody. *AIAA Journal*, 52:1967–1979, 2014.
- [14] R. Pain, P.-E. Weiss, S. Deck, and J.-C. Robinet. Large scale dynamics of a high Reynolds number axisymmetric separating/reattaching flow. *Physics of Fluids*, 31(12):125119, December 2019.
- [15] R. Verzicco, J. Mohd-Yusof, P. Orlandi, and D. Haworth. Large eddy simulation in complex geometric configurations using boundary body forces. *AIAA Journal*, 38(3):427–433, 2000.
- [16] P.-E. Weiss and S. Deck. Control of the antisymmetric mode ($m = 1$) for high Reynolds axisymmetric turbulent separating/reattaching flows. *Physics of Fluids*, 23(095102), 2011.
- [17] P.-E. Weiss and S. Deck. ATAC : étude des charges latérales sur la configuration Ariane 5 lisse NLR3D avec les attaches des boosters (RT 2/17121 DAFE/DAAP - RT-NT-418-17121-ONER-02). Octobre 2012.
- [18] P.-E. Weiss and S. Deck. Simulation numérique des charges instationnaires sur un arrière-corps de type Ariane 5 muni de bielles au moyen dune technique de frontières immergées. (RT 2/23806 DAAP - RT-NT-418-1401-ONER-02). Septembre 2015.
- [19] P.-E. Weiss and S. Deck. ZDES of the flow dynamics on an Ariane 5-type afterbody with and without struts. *6th European Conference for Aerospace Sciences, Flight Physics, Launcher Aerodynamics*, 2015.
- [20] P.-E. Weiss and S. Deck. Towards an efficient and robust numerical strategy for fast aerodynamic performance prediction on launch vehicles. *7th European Conference for Aerospace Sciences, Flight Physics, Launcher Aerodynamics*, 2017.
- [21] P.-E. Weiss and S. Deck. On the coupling of a zonal body-fitted/immersed boundary method with ZDES: application to the interactions on a realistic space launcher afterbody flow. *Computers & Fluids*, 176:338–352, 2018.
- [22] P.-E. Weiss and S. Deck. ZDES of an Ariane 6 PPH configuration with incidence angle using Zonal Immersed Boundary Conditions. *8th European Conference for Aerospace Sciences, Flight Physics, Launcher Aerodynamics*, 2019.
- [23] P.-E. Weiss, S. Deck, J. C. Robinet, and P. Sagaut. On the dynamics of axisymmetric turbulent separating/reattaching flows. *Physics of Fluids*, 21(075103), 2009.